Meas. Sci. Technol. **18** (2007) 2809–2816 doi:10.1088/0957-0233/18/9/010

Achieving sub-millimetre precision with a solid-state full-field heterodyning range imaging camera

A A Dorrington[1], M J Cree[1], A D Payne[1], R M Conroy[1] and D A Carnegie[2]

[1] Department of Engineering, University of Waikato, Private Bag 3105, Hamilton, New Zealand
[2] School of Chemical and Physical Sciences, Victoria University of Wellington, PO Box 600, Wellington, New Zealand

Received 18 October 2006, in final form 10 May 2007
Published 20 July 2007
Online at stacks.iop.org/MST/18/2809

Abstract
We have developed a full-field solid-state range imaging system capable of capturing range and intensity data simultaneously for every pixel in a scene with sub-millimetre range precision. The system is based on indirect time-of-flight measurements by heterodyning intensity-modulated illumination with a gain modulation intensified digital video camera. Sub-millimetre precision to beyond 5 m and 2 mm precision out to 12 m has been achieved. In this paper, we describe the new sub-millimetre class range imaging system in detail, and review the important aspects that have been instrumental in achieving high precision ranging. We also present the results of performance characterization experiments and a method of resolving the range ambiguity problem associated with homodyne and heterodyne ranging systems.

Keywords: range, distance, heterodyne, full-field, three-dimensional, imaging, metrology, sub-millimetre, millimetre, precision

1. Introduction

Methods for the capture of three-dimensional images have been researched for some time now, with a great variety of approaches developed and applied to a wide variety of applications. Such applications include machine vision, surface profiling, surveying, metrology, real-time multi-media integration and three-dimensional recordings of objects and artefacts. Each application has unique requirements for measurement precision, speed and coverage. In general, the methods that are available for three-dimensional image capture can be divided into the four broad categories of laser scanning, stereo vision, structured light and imaging lidar systems.

The first three categories are well established and described in detail in many publications elsewhere [1–5]. However, the final category of imaging lidar is a comparably new field with a relatively small number of systems demonstrated with varying degrees of success [6–14]. Despite a variety of implementations, these systems have common operating principles and similar hardware configurations, and all generate a digital photograph-like output that contains distance (or range) information for every pixel in the image as well as greyscale or colour information.

We have developed a full-field solid-state lidar based range imaging system, called the Range Imager, that is capable of sub-millimetre ranging precision. Sub-millimetre precision has been achieved through continued and incremental improvements in electronics and signal processing [1, 17, 18] from an earlier system only capable of ranging precisions in the order of centimetres [12]. In this paper, we briefly review the principles of imaging lidar systems, then describe our Range Imaging system paying attention to the key factors essential for obtaining sub-millimetre precision.

2. Imaging lidar systems

Imaging lidar systems operate by illuminating a scene with intensity-modulated light and imaging with a gain modulation camera. This gain modulation is usually performed with a (non-mechanical) shuttering mechanism in front of the camera or built into a custom sensor. The major differences between imaging lidar systems arise in the modulation control signals used for the light source and the shuttering mechanism, and the implementation of the shuttering system itself. The most common shutter implementation is an image intensifier with high-speed photo-cathode modulation capability [6–9]. Image intensifiers are popular as high-speed shutters because they are one of the few technologies capable of image gain modulation up to 100 MHz; nevertheless, they suffer from a number of disadvantages including relatively poor spatial resolution and the need for high voltage (up to 7 kV) power supplies. Therefore, there is a move to integrate high-speed shuttering capabilities in custom image sensors. A number of these types of sensors have been demonstrated, but they are currently limited in spatial resolution [13–16].

The modulation philosophies used can be grouped into the three main categories of pulsed, homodyne and heterodyne. In the pulsed systems, both the illumination source and the high-speed shutter are controlled with a single pulse in the nanoseconds region. Range is represented directly as a grey level and is limited by the dynamic range of the sensor. Complicated pulse control systems can be used to select a depth region of interest, and provide higher precision over that narrow region.

Homodyne systems use a continuous square, sinusoidal or triangle wave modulation on the illumination and shutter generally in the 10–100 MHz region. Propagation delay to objects in the scene causes a phase change in the illumination modulation envelope, resulting in a change in grey level brightness. Some decoding is required to derive actual range values from brightness, and often multiple measurements are acquired at different relative phases of the modulation signals to perform quadrature or phase-shift-keying type decoding. Because phase is cyclic, range ambiguities (the same reading for several different ranges) occur at multiples of half of the wavelength of the modulation signal.

In heterodyne systems the modulation frequencies applied to the illumination and shutter differ slightly in frequency [1, 12]. A beat frequency equal to the difference between the modulation frequencies is produced after the camera shutter (appearing as a 'flashing' image), where objects at different distances have different phase values. Every pixel in the image has the same beat frequency, but different phase values that represent range. The range d for each pixel can be determined by calculating the beat signal phase ϕ from the intensity time history, and applying the relationship [22]

$$d = \frac{\phi}{4\pi}\frac{c}{f_{\mathrm{m}}} = \frac{\phi\lambda_{\mathrm{m}}}{4\pi} \qquad (1)$$

where f_{m} is the modulation frequency, λ_{m} is the modulation signal wavelength and c is the speed of light. The heterodyne approach with phase detection is used by the Range Imager and is described in more detail in [1].

For pulse and homodyne systems, pixel brightness is not only a function of range but is also a function of background lighting and object colour and/or surface reflectance. Compensation procedures are required to remove these disruptive effects resulting in a reduced dynamic range available in the image sensor, thereby limiting the range measurement resolution and precision. Better ranging precision is generally achieved with heterodyne systems because range is determined as a function of temporal variations in the detected signal rather than intensity variations.

Table 1. Range Imager typical operating configuration and system performance.

Characteristic	Value
Configuration settings:	
Imaging resolution	512 × 512 pixels
Modulation frequency	65 MHz
Range measurement time	10 s
Video frame rate	29 fps
Acquired video frames	290
Beat frequency	1 Hz
Lens focal length	80 mm
Lens aperture	4.5 *f*-number
System performance:	
Minimum operating distance	1 m
Ranging precision 1σ (best case)	0.6 mm
Field of view	18°

By virtue of the distance determination through beat signal phase measurement, the heterodyne approach used here is less sensitive to disruptions from surface scattering properties and background illumination than the traditional homodyne method. Because the homodyne approach determines distance though grey levels in the image, a change in returned intensity will have a direct impact on the distance determination. With a temporal approach to distance determination, any changes to returned intensity or grey level have only an indirect influence. A change in the signal level will not directly affect the signal phase, and with the heterodyne approach, will only affect distance determination through factors such as a change in signal-to-noise ratio or quantization distortion.

Furthermore, the nature of the temporal processing requires heterodyne systems to acquire between one and two orders of magnitude more images than pulsed or homodyne systems, providing more data to process and thereby contributing to the higher obtainable precision.

3. The University of Waikato range imager

The Range Imaging Group at the University of Waikato (Hamilton, New Zealand) have developed a 3D imaging system based on the heterodyne ranging approach called the Range Imager. The heterodyne approach was chosen because it exhibits better ranging precision performance. The system configuration is flexible with settings such as acquisition time, imaging resolution and modulation frequency adjustable to suit a given application. For most experimental work, the settings are generally kept constant as summarized in table 1. Table 1 also shows the system performance exhibited under these conditions.

The system has been assembled predominantly using off-the-shelf components. Previously we have shown that the two most important factors for obtaining sub-millimetre precision are high operating frequency and good signal-to-noise ratio [1]. From a practical perspective, avoiding CCD image smear and frequency locking the camera frame rate to the beat signal are also important in achieving high ranging precision [17, 18]. Improving these important factors has guided both design

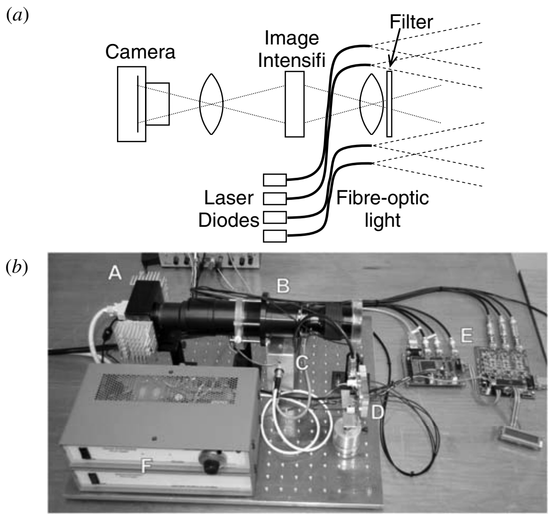

Figure 1. Optical hardware (*a*) schematic and (*b*) photograph showing the (A) digital video camera, (B) image intensifier, (C) intensifier driver, (D) laser diodes and driver, (E) signal generation electronics and (F) power supplies.

emphasis and the choice of the off-the-shelf components. In the description that follows, we group the components of the system into three primary hardware sub-systems: imaging, illumination, and signal generation and drive electronics. This is followed by a description of the control and processing software.

3.1. Hardware sub-systems

3.1.1. The imaging sub-system. The imaging sub-system (shown in figure 1) consists of four components: a digital video camera for image acquisition, an image intensifier used as the high-speed shutter, and two lenses, one to image the scene on to the intensifier input and another to couple the intensifier output onto the camera.

Because heterodyne ranging requires the analysis of time varying signals, it is necessary to process a video sequence of the scene. A Dalsa Pantera TF 1M60 digital video camera, attached to a Camera-link frame grabber card (PC-Camlink, Coreco Imaging Inc) is used. This camera has the advantages of

- 12 bit dynamic range, providing a high signal-to-noise ratio for good phase determination precision [1];
- 100 Hz frame rate at 512 × 512 resolution (2 × 2 binning mode);
- External frame trigger with low jitter for synchronized frame acquisition control.

The high-speed shuttering mechanism is implemented with a 25 mm diameter single micro-channel plate (MCP) generation II image intensifier (Photek Ltd, East Sussex, UK), configured for photocathode modulation. A custom-made power supply provides a 5.5 kV screen voltage, the 0–700 V MCP voltage and a 67 V photocathode bias voltage. The screen and bias voltages are preset, while the gain of the intensifier, controlled by the MCP voltage, is adjustable either manually from a front panel dial or automatically from the controlling computer.

Image intensifiers are conventionally operated with a photocathode voltage of −200 V in the 'on' state; however, to achieve modulation frequencies approaching 100 MHz, a photocathode drive of −40 V to +10 V swing was chosen. Such a low voltage has the disadvantages of lower gain and reduced limiting spatial resolution and is a compromise with the electronic practicality of driving high voltages at high frequencies into a capacitive load (around 60 pF). Fortunately, the relative per-voltage improvement in these factors diminishes at drive levels larger than −40 V [19].

The photocathode modulation signal is provided by a custom driver circuit [20]. The input signal is passed through a comparator to create a square wave, and then through digital logic to selectively enable/disable the circuit for long or short periods (down to single pulses) to reduce power dissipation. A National Instruments LM2412 CRT driver is used to amplify the logic level signal to 50 V peak-to-peak which is combined with a DC offset voltage in bias-T to drive the photocathode. All three driver channels have been combined in parallel through current sharing resistors to drive the relatively high capacitance load. The output rise and fall times are 3.5 ns, providing bandwidth of 100 MHz. Using this arrangement and a square wave drive has many advantages, including

- fast traverse through the poor resolution low voltage photocathode drive regions;
- asymmetrical on/off voltages for better efficiency photocathode drive;
- single cycle control of the intensifier, for example, to turn off the intensifier during CCD frame transfer to prevent image smear.

A standard Nikon F-mount lens adaptor is built into the image intensifier housing for ease of lens selection and replacement. The majority of our imaging to date has been through a 80–200 mm zoom lens with an f-number of 4.5. A 645 nm long pass filter is employed to reject background lighting (model LP645-52, Midwest Optical Systems, Palatine, IL). In this region the response of the photocathode is already decreasing at longer wavelengths, so the combination of photocathode response and long-pass filter forms a band-pass-type response.

The image intensifier to camera coupling is performed with a low *f*-number ($f/\# = 1.0$) lens with a working distance of approximately 15 mm (model S5LPJ1035 & S5LPJ1871, Sill Optics, Wendelstein, Germany). The small *f*-number and close working distance significantly improve the optical efficiency of the intensifier to camera coupling. Fibre-optically coupling a smaller diameter image intensifier to the camera would be more efficient, but for the purposes of this prototype system the flexibility of lens coupling was more attractive.

3.1.2. The illumination sub-system. The illumination sub-system uses a bank of four 80 mW laser diodes (Mitsubishi ML120G21) to illuminate the scene. They are independently driven by voltage controlled current switches (iC-HK from iC-Haus), which are capable of current modulation up to 155 MHz. Like the image intensifier driver, the input signal is fed through a comparator to generate a square wave that is buffered to provide an identical CMOS level output to each iC-HK chip. A fibre-optic cable is used to deliver the light

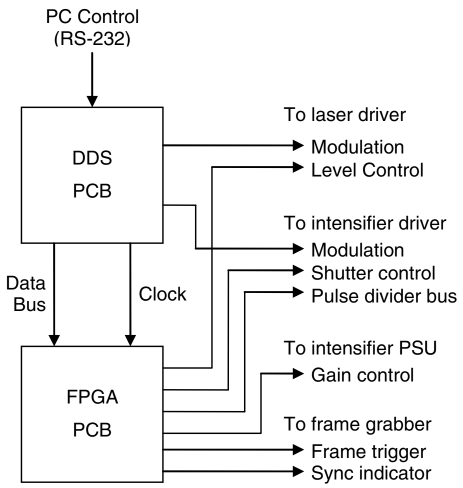

Figure 2. Schematic diagram of the electronics sub-system showing the two signal generation boards (DDS and FPGA) and their signal connections.

from each laser to the imaging head, where lenses are used to provide control over the divergence of the illumination. This arrangement provides both coaxial illumination and mode-scrambling of the laser light for a significantly more homogeneous and circular illumination pattern.

Four individual laser diodes are used both to provide a high level of illumination for higher signal-to-noise ratio and to help reduce shadowing effects by a circular illumination arrangement around the main imaging lens. With illumination sources diametrically opposed about the optical axis, the shadows caused by object obstructing illumination from one source location are illuminated by light from its complementary source location.

The laser diodes do not have an integrated photodiode within the package, so are driven in constant current mode with care taken to ensure that the lasers are not overdriven, especially during turn-on and warm-up. The computer control software can adjust the laser output and perform an automated safe warm-up sequence via an analogue input on the laser driver hardware.

3.1.3. The signal generation sub-system. The signal generation sub-system provides functionality to generate all necessary signals for control of the system. As shown schematically in figure 2, two main circuit boards are used, one containing the analogue output direct digital synthesizer (DDS) signal generators and microprocessor control circuits, and the other containing a field programmable gate array (FPGA) digital circuit generating mostly digital control signals. The FPGA board contains two digital-to-analogue converters to provide analogue outputs for laser level control and intensifier gain control.

Because ranging precision is proportional to the wavelength of the modulation signal (see equation (1)), operating at the highest possible modulation frequency provides the best possible precision. Previous experiments have clearly shown this inverse relationship between modulation frequency and range measurement precision [1]. The same experiments have demonstrated a phase measurement precision of 1.6 mrad almost irrespective of operating frequency with optimal lighting and surface scattering properties. As the returned signal level drops so does the signal-to-noise ratio and phase precision is impacted. These same experiments have shown that phase determination of better than 2.5 mrad is maintained with returned light down to 40% of optimal.

Difficulty arises with modulation frequencies up to 100 MHz and beat frequencies of singles of Hertz because relative stability in the signal generators of more than nine orders of magnitude is required. This problem is solved by employing a DDS architecture, which digitally generates a sine wave using a lookup table and a DAC with all output signals derived from a single common clock. The signals are said to be frequency-locked, and although the signal frequencies may drift in unison, the frequency difference between the two modulation signals remains suitably consistent. Our custom-designed signal generator employs three DDS ICs (Analogue Devices AD9952) interfaced to a microcontroller (Atmel 89LS8252), and can generate output signals with 0.093 Hz frequency resolution.

As shown in figure 2, an FPGA logic circuit is used to perform a number of digital signal generation functions. Most importantly, the camera frame rate is derived directly from the input clock for the DDS. This frequency locks the camera frame rate to the beat signal and allows simplified inner-product range processing (explained below). A zero-phase synchronization reference pulse, which is asserted when all three DDS output signals are in phase, is also generated to enable calculation of absolute distance as opposed to relative distance.

An unfortunate disadvantage of frame-transfer CCD sensors is the presence of image smear. This problem arises because the image continues to be integrated while being transferred from the sensing area into the storage area of the CCD [23]. The transfer process is usually very fast and therefore any light collected during the transfer process is negligible compared to that collected during the integration time, and does not normally present a problem for images used for visual purposes. In heterodyne imaging however, the small amounts of pixel-to-pixel beat signal contamination caused by image smear can have a significant impact on measurement precision [17]. To completely avoid the problem of image smear, a shuttering signal to gate the photocathode of the intensifier is generated to ensure the intensifier is turned off during the CCD frame transfer operation.

3.2. Processing and control software

The functionality of the control software can be divided into the three areas of acquisition control, data processing and data visualization. Each of these areas is described below.

3.2.1. The acquisition control. The acquisition control system has three primary modes of operation: disabled, preview mode and measurement mode. In disabled mode, all systems remain in a running state except for the image intensifier which is switched off to avoid excess power dissipation and over-heating of the equipment. Preview mode is used to view the scene through the imaging system for scene setup and adjustments of the optics such as focusing. The image intensifier is operated at a low modulation frequency (of around 1 MHz) to avoid excess power dissipation thereby enabling extended periods of thermally safe operation. A continual process of auto-gaining is performed to ensure optimal display of the imaged scene.

In measurement mode image sequences are captured to memory at full speed without any display on the monitoring screen. Before the capture is started, an auto-gain procedure is performed to find the optimal gain level. The intensifier is modulated at the full speed (up to 95 MHz), but because significant amounts of power are dissipated by the intensifier driver circuit and also by the photocathode itself, operation can only by sustained for 30 s or so. The data are then either directly processed on-line in real time to generate depth data or saved to disk as an audio–video interleave (AVI) file for off-line processing.

3.2.2. The image sequence processing. The image sequence processing performs range determination by calculating the phase of the time-varying beat signal for each pixel and using equation (1). To perform this phase determination, we use both a fast Fourier transform (FFT) approach and more recently, a faster and simpler inner-product approach. These processing algorithms are performed on the entire video sequence of captured frames subsequent to the image sequence acquisition process.

In the FFT approach a sub-selection of the brightest 4000 pixels in the video sequence is used to estimate the beat frequency [22]. The brightest pixels are used to give the best signal-to-noise ratio, and hence the best estimation of beat frequency. Four times zero padding plus quadratic interpolation about the peak in the frequency spectrum provides sub-bin beat frequency estimation precision. Then the full video sequence is Fourier analysed with four times zero padding and linear interpolation in the frequency domain at the previously estimated beat frequency to provide the phase of the beat signal. This algorithm is robust to changes in video frame rate or beat frequency and was necessary in previous versions of the system that did not have the frame rate frequency locked to the beat frequency.

With the improvements in hardware described above the drive signals can be arranged so that the beat signal falls completely within a frequency bin; hence an inner-product approach (or direct calculation of the known single frequency bin) can be used. In order to get the best performance from the inner-product processing, it is important to ensure (1) an integer number of beat cycles in the acquisition period and (2) a prime number of samples in the acquisition period [18]. The second condition arises because nonlinearities of the image intensifier introduce harmonics to the beat signal which can be aliased onto, or very near, the fundamental frequency. It is not possible to temporally filter the light signal from the image intensifier before sampling; thus aliasing cannot be avoided. By choosing a prime number of samples in the acquisition period, the likelihood of aliasing harmonics onto the fundamental is greatly reduced.

A comparison has been performed to quantify the relative performance of these two processing approaches. The single-pixel measurement precision was determined individually for a set of eight video sequences by acquiring a range image of a flat panel and finding the standard deviation of the residuals between the measured data and a least-squares planar fit for several small regions of the image (20×20 pixels). A 20×20 region provides a sufficient number of pixels to calculate the standard deviation without allowing surface flatness non-uniformities to influence the results. As expected, there was very little difference between the two algorithms, averaging 0.03% and never exceeding 0.15%. In every case however, the inner-product algorithm was approximately 11 times faster than the FFT algorithm. Consequently, we use the inner-product algorithm except for unusual circumstances such as a degraded video sequence, where robustness to missing data or dropped frames is advantageous.

Both algorithms on their own can only provide relative phases. A zero-phase reference is instead provided by the signal generation electronics to indicate which video frame has its start of integration synchronized with a zero-phase difference in the modulation signals. This reference is encoded in the bottom-left pixel of each image. The reference does not interfere with the scene reconstruction as it is outside the viewable aperture of the image intensifier. The processing algorithm uses the reference zero phase to provide absolute phase values. A further offset correction is made to compensate for the electronic and optical delays in the system, which are determined by calibration.

It is well known that homodyne and heterodyne image ranging suffer from an ambiguity problem that arises from the cyclic nature of the modulation signal. Ambiguity arises if the time delay causes a phase change larger than one complete cycle (2π), meaning a particular phase measurement could represent several possible distance measurements separated by multiples of one half wavelength of the modulation envelope.

Consider the example illustrated in figure 3. The modulation frequency of 100 MHz has a wavelength of approximately 3 m; thus the ambiguity distance is half of the wavelength or 1.5 m for this example. This means that a phase measurement of π radians could represent the candidate distance measurements (in metres) of 0.75, 2.25, 3.75, 5.25 and so on. To resolve this ambiguity, a second measurement of the same scene could be performed at a slightly different modulation frequency. For example, now consider the modulation frequency 93.75 MHz with an ambiguity distance of 1.6 m. A phase measurement of $(11/16)\pi$ represents candidate distances (in metres) of 0.55, 2.15, 3.75, 5.35 and so on. Note that there is only one common candidate distance to both sets, and the actual distance can be confirmed as 3.75 m.

Actual measurements contain noise, so there will not be an exact match of candidate distances for a pair of measurements. To resolve ambiguities, we find the minimum difference for every combination of candidate distances. The ambiguity-resolved distances for the two measurements are then averaged to find an unambiguous distance, which achieves a factor of root two better precision. Figure 4 shows measurements of two objects and the back wall as (a) the intensity data, as well as an example of a range image measurement processed (b) without ambiguity processing and (c) with ambiguity resolved. The objects are intentionally separated by a distance close to the ambiguity distance, and appear close to each other without ambiguity processing. With ambiguity resolved it is seen that these objects are in fact at substantially different ranges.

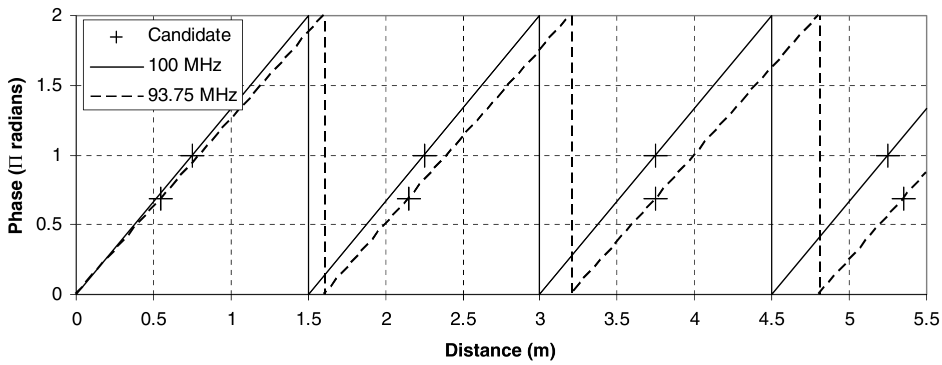

Figure 3. Resolving ambiguity example. Simulated phase versus distance is shown for two modulation frequencies with candidate distances for two hypothetically measured phases (π and $(11/16)\pi$ radians).

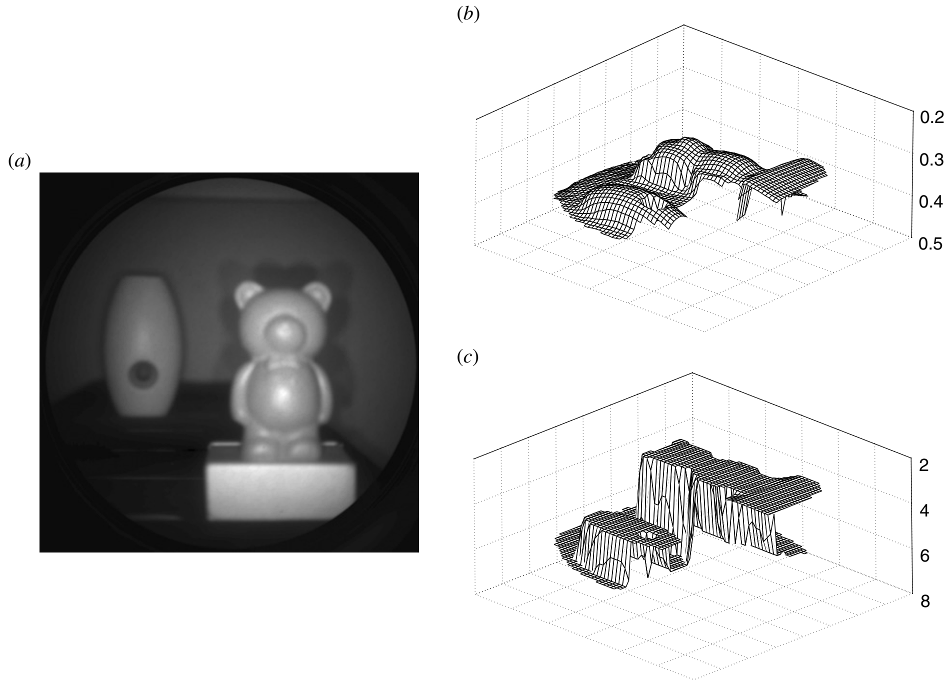

Figure 4. Ambiguity resolved range measurements. (*a*) Intensity data from ranger acquisition showing two objects, a bear standing on a box and a vase and the back wall. (*b*) Range data without ambiguity processing. (*c*) Range data with ambiguity processing. Vertical scale on wire frame plots is the distance from the camera in metres.

The objects appear flat in the ambiguity-resolved plot simply because of the scale change on the vertical axis. Closer inspection of the data reveals all of the detail is present. As evident in the intensity image data, the table is covered with a black cloth, and hence insufficient light is returned to make a measurement, so the table does not appear in the range mesh plots. Note that the data plotted in figure 4 have been spatially sub-sampled for clarity of the mesh.

Although it has not been implemented yet, there is the potential to perform both range measurements simultaneously. This can be achieved by modulating the illumination and the shuttering with a superimposition of the two modulation frequencies. By tuning the frequency differences for each set of modulation frequencies, two separate beat signals can be obtained. The Fourier-type analysis used allows independent processing of these beat signals, thereby providing the two independent measurements. Care must be taken when selecting the beat frequencies, paying attention to the aliasing criteria described above, to not only avoid harmonic interference within a given beat frequency, but also between beat frequencies.

4. Characterization experiments

A set of experiments has been performed to determine the operational parameters of the range imaging system. The first experiment was designed to determine how the measurement precision changes with distance to viewed objects. The precision was determined by imaging a diffuse while flat panel and performing planar fits to small regions (20 × 20 pixels) of the measured range image. The standard deviation of the residue of the fit provides the precision. Figure 5 shows the results from two individual experiments, one with the auto-gain system enabled and one with it disabled. When auto-gain

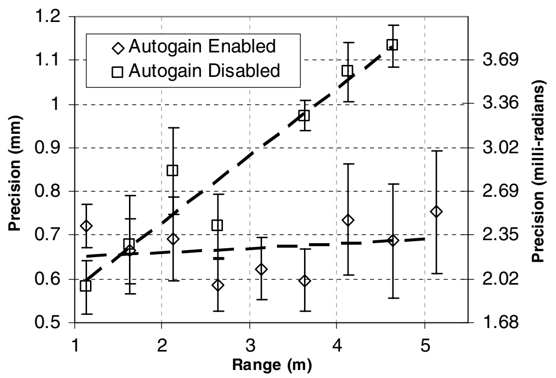

Figure 5. Measurement precision versus object range for simulated small and large depths of field.

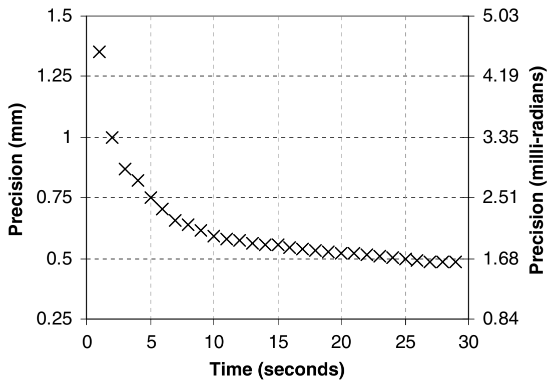

Figure 6. Measurement precision versus measurement time.

is enabled, we are effectively simulating a small depth of field, where the object being measured occupies a relatively small distance variation in range. With auto-gain disabled, the gain was optimized for the closest object and remained the same for all measurements. This effectively simulates the situation where a scene being imaged contains objects at all distances over a large depth of field.

In the small depth of field situation, sub-millimetre precision is maintained and changes only slightly over the 1–5.5 m distance range. This indicates that the loss of light due to the inverse square law is adequately compensated for by the gain adjustment in the image intensifier. It also indicates that the photon noise has minimal impact on precision, and that other noise sources are dominant. For the case of large depth of field, the precision worsens as distance to the object increases and the collected light decreases. There appears to be a predominantly linear relationship between distance and precision. All of these measurements were performed at 65 MHz modulation frequency, 29 Hz frame rate and with a 10 s acquisition.

The system continues to function beyond the 5.5 m range shown in figure 5, but a detailed analysis of performance in this region has so far been hampered by physical space restrictions. As the operating distance is increased, the retuned signal level drops causing a reduction in the signal-to-noise ratio, and hence precision. Provisional measurements performed with the aid of a mirror to simulate a longer measurement path show a precision of approximately 2 mm at an operation distance of 12 m.

A second experiment was performed to determine the relationship between precision and acquisition time (the number of acquired video frames). This was achieved by acquiring a single long acquisition video sequence, and processing with increasing numbers of video frames, thereby simulating increasing acquisition times without the influence of acquisition-to-acquisition uncertainties. The results are graphed in figure 6, which shows an expected improvement in precision with increasing acquisition time; however, acquisitions longer than 10 s show diminishing returns with respect to precision. This experiment was performed at 65 MHz modulation rate and 29 Hz frame rate.

5. Measurement example

To visually demonstrate the capability of our range imaging system, we present an example measurement of a garden gnome. This object provides a good demonstration because of its variety of colours and reflectance characteristics, and because it contains regions of smooth surfaces and regions of detailed surface texture. Figure 7 shows both photographs of the gnome and a plot of the range image captured. The range

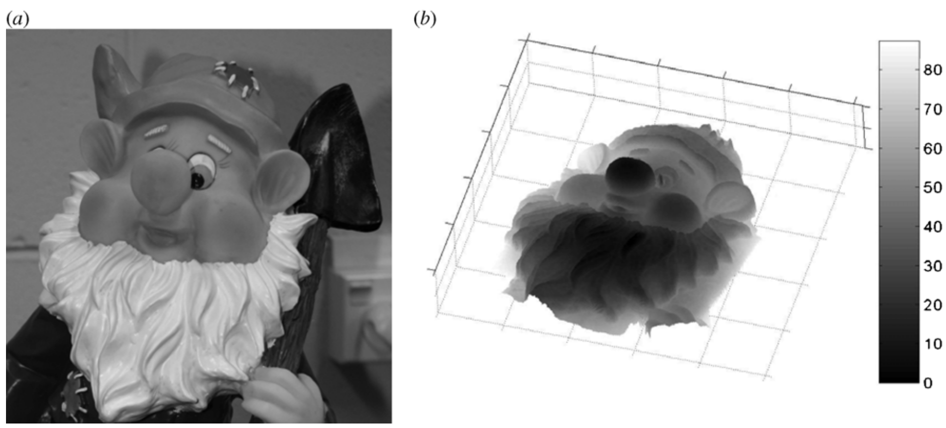

Figure 7. Example measurement of a multi-coloured object showing both (*a*) a photograph of the object and (*b*) a plot of the range image scaled in millimetres.

image plot shows relative distance in millimetres away from the camera on a grey scale. Note that the captured range data faithfully represent the object except for a small region in the gnome's eye. This error in the eye is caused by a specular refection that saturates the camera resulting in errors in the phase determination algorithm. For this capture, the system was configured with the same parameters shown in table 1.

6. Conclusion

We have developed a solid-state full-field intensity modulated heterodyne based range imaging system. This system is capable of acquiring range data for every pixel in a scene simultaneously with a one-sigma precision of less than 1 mm out to more than 5 m. The system includes mechanisms for determining absolute (rather than relative) distance measurements, and for resolving measurement ambiguity. Also included is synchronized signal generation for frequency locking the measurement signals to the sample clock allowing the implementation of high speed inner-product phase determination processing. During development, we identified a number of aspects and criteria that are important in achieving high measurement precision. These aspects include the ability to acquire image sequences of the heterodyne beat signal with a high signal-to-noise ratio, operating with high modulation frequencies, avoiding CCD image smear and careful choice of sample rate and beat signal frequencies.

Further work is required to extend the discussion of range measurement precision presented in this paper to three-dimensional object space measurement accuracy. Converting range image data into three-dimensional measurements requires a perspective projection process, such as that used in applications such as Photogrammetry. To perform a successful perspective projection, calibration procedures need to be developed for imaging and ranging distortions, such as radial lens distortion, light source & imaging geometric distortions and image intensifier irising distortions.

Although not yet tested with other full-field range imaging hardware, we expect that the heterodyne techniques described here (and in our previous works [1, 17, 18, 20–22]) could easily be implemented in alternative hardware. We anticipate a similar improvement in ranging precision when converting existing homodyne systems into a heterodyne approach.

Acknowledgments

Funding for this research was provided in part by the Foundation for Research, Science and Technology (New Zealand) through the New Zealand Science and Technology Postdoctoral fellowship, and the Pre-seed Accelerator Fund.

References

[1] Dorrington A A, Carnegie D A and Cree M J 2006 Towards 1-mm depth precision with a solid state full-field range imaging system *Proc. SPIE* **6068** 60680K

[2] Besl P J 1988 Active range imaging sensors *Mach. Vis. Appl.* **1** 127–52

[3] Blais P J 2004 Review of 20 years of range sensor development *J. Electron Imaging* **13** 231–40

[4] Marr D and Poggio T 1976 Cooperative computation of stereo disparity *Science* **194** 282–7

[5] Atkinson K B 1996 *Close Range Photogrammetry and Machine Vision* (Caithness, Scotland: Whittles Publishing)

[6] Gvili R, Kaplan A, Ofek E and Yahav G 2003 Depth keying *Proc. SPIE* **5006** 564–74

[7] Busck J and Heiselberg H 2004 Gated viewing and high-accuracy three-dimensional laser radar *Appl. Opt.* **43** 4705–10

[8] Anthes J P, Garcia P, Pierce J T and Dressendorfer P V 1003 Non-scanned LADAR imaging and applications *Proc. SPIE* **1936** 11–30

[9] Christie S, Hill S L, Bury B, Gray J O and Booth K M 1995 Design and development of a multi-detecting two-dimensional ranging sensor *Meas. Sci. Technol.* **6** 1301–8

[10] Stann B, Giza M, Robinson D, Ruff W, Sarama S, Simon D and Sztankay Z 1999 A scannerless imaging ladar using a laser diode illuminator and FM/cw radar principles *Proc. SPIE* **3707** 421–48

[11] Kawakita M *et al* 2004 High-definition real-time depth-mapping TV camera: HDTV axi-vision camera *Opt. Express* **12** 2781–94

[12] Carnegie D A, Cree M J and Dorrington A A 2005 A high-resolution full-field imaging system *Rev. Sci. Instrum.* **76** 083702

[13] Gokturk S B, Yalcin H and Bamji C 2004 A time-of-flight depth sensor—system description, issues and solutions *Proc. Conf. Computer Vision and Pattern Recognition Workshop* vol 3 p 35

[14] Gulden P, Vossick M, Heidi P and Schwarte R 2002 Novel opportunities for optical level gauging and 3-D-imaging with the photoelectronic mixing device *IEEE Trans. Instrum. Meas.* **51** 679–84

[15] Buttgen B *et al* 2006 High-speed and high-sensitive demodulation pixel for 3D-imaging *Proc. SPIE* **6056** 605603

[16] Ushinaga T, Halin I A, Sawada T, Kawahito S, Homma M and Maeda Y 2006 A QVGA-size CMOS time-of-flight range image sensor with background light charge draining structure *Proc. SPIE* **6056** 605604

[17] Dorrington A A, Cree M J and Carnegie D A 2005 The importance of CCD readout smear in heterodyne imaging phase detection applications *Proc. Image and Vision Computing New Zealand* pp 73–8

[18] Dorrington A A, Cree M J, Carnegie D A and Payne A D 2005 Selecting signal frequencies for best performance of Fourier-based phase detection *Proc. 12th Electronics New Zealand Conf.* pp 189–93

[19] Bosch L A 1995 Dynamic uses of image intensifiers *Proc. SPIE* **2551** 159–72

[20] Payne A D, Carnegie D A, Dorrington A A and Cree M J 2006 Full field image ranger hardware *Proc. Third IEEE Int. Workshop on Electronic Design, Test & Applications* pp 263–8

[21] Dorrington A A 2004 Range sensing system *International Patent* PCT/NZ2004/000070

[22] Cree M J, Dorrington A A and Carnegie D A 2005 A Heterodyning Range Imager *Proc. Ninth IAPR Conf. Machine Vision Applications* pp 80–3

[23] Holt G C 1998 *CCD Arrays Cameras and Displays* 2nd edn (Bellingham, WA: SPIE Optical Engineering Press)